ACS APPLIED MATERIALS & INTERFACES

Research Article

www.acsami.org

Influence of the Ionic Functionalities of Polyfluorene Derivatives as a Cathode Interfacial Layer on Inverted Polymer Solar Cells

Rira Kang,[†] Seung-Hwan Oh,[§] and Dong-Yu Kim*[,†,‡]

[†]Heeger Center for Advanced Materials (HCAM), School of Materials Science and Engineering and [‡]Department of Nanobio Materials and Electronics, Gwangju Institute of Science and Technology, 1 Oryong-Dong, Buk-Gu, Gwangju 500-712, Republic of Korea

[§]Radiation Research Division for Industry & Environment, Korea Atomic Energy Research Institute (KAERI), 29 Geumgu-gil, Jeongup-si, Jeollabuk-do 580-185, Republic of Korea

Supporting Information

ABSTRACT: In this work, we synthesized water-soluble polyfluorene derivatives (WPFs) with anionic and/or cationic side chains, which were used as an indium tin oxide (ITO) cathode interfacial layer in inverted polymer solar cells. Three WPFs (WPFN+, WPFZW, and WPFS-) were obtained via Suzuki coupling reactions. Their solubility in polar solvents allowed the WPFs to be used as interfacial layers in inverted polymer solar cells (I-PSCs). Among the WPF-modified ITO electrodes, WPFN+ (with ammonium side chains)-modified ITO can be used as a cathode for electron extraction, while WPFS- (with sulfonate side chains)-modified ITO cannot extract electrons in I-PSCs based on poly(3-hexylthiophene): [6,6]-phenyl-C_{61}-butyric acid methyl ester (P3HT:PC_{61}BM). The electron extraction of WPF-modified ITO can mainly be attributed to the different dipole formations at the WPF/ITO interfaces, based on the types of ionic groups on the side chains of the polyfluorene. In addition, we observed that the extent of ITO work-function modification was not always exactly correlated with the device performance based on the results obtained using a WPFZW (with ammonium and sulfonate side chains)-modified ITO electrode.

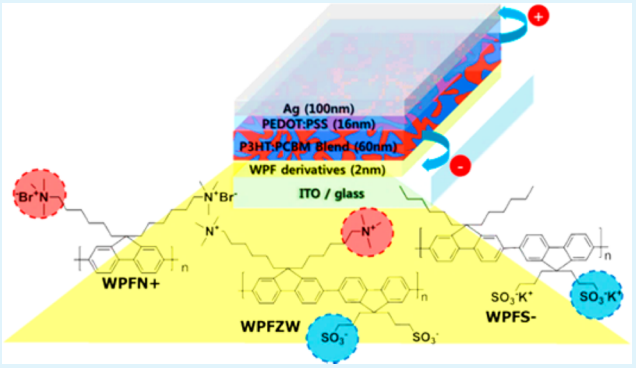

KEYWORDS: *conjugated polyelectrolytes, polyfluorene, dipole layer, work-function modification, interfacial layer, inverted polymer solar cells*

1. INTRODUCTION

Conjugated polyelectrolytes (CPEs) include both a conjugated main chain and side chains that consist of either ionic or polar groups. The conjugated main chains yield typical organic semiconducting properties such as intra-chain and/or inter-chain energy transfer, large optical densities, and fluorescence resonance transfer.[1−6] The ionic or polar groups of the side chains render conjugated polymers soluble in water and other polar solvents such as dimethylsulfoxide (DMSO), dimethyl-formamide (DMF), and methanol (MeOH), and their compensating ions can migrate under external electric fields.[1−6] These ionic functionalities make CPEs good candidates for the interfacial layer material of solution-processed multilayer organic electronic devices,[7,8] because they prevent intermixing with the underlying layers, and they allow the subsequent coating of the organic soluble layers. Furthermore, they modify the work-function of adjacent metal electrodes arising from the surface dipole at the CPE/metal interface.[9−17,19,20]

By forming effective surface dipoles at the CPE/metal interface, a number of CPEs have been investigated for use as an interfacial layer for electron transport in polymer light emitting diodes (PLED),[1,13,17,19] in conventional polymer solar cells (PSCs),[1,9,12,13,17,20] and in inverted polymer solar cells (I-PSCs).[10,11,13−16,34] The formation of surface dipoles shifts the vacuum level at the CPE/cathode interface and lowers the work-function of cathode electrodes such as Ag, Al, Cu, and Au, which have a high work-function and are stable in conventional PSCs.[13] CPEs also form favorable surface dipoles at the CPE/ITO interface in I-PSCs when using ITO as a cathode electrode and high work-function metals as anode electrodes. In other words, ITO as a cathode electrode sufficiently collects electrons when using CPEs as the ITO cathode interfacial layer (cIFL).[10,11,14−16] Recently, highly efficient PSCs have demonstrated a certified efficiency of 8.4% using an inverted structure and CPEs (PFN-Br) as an ITO cIFL.[15] The use of CPEs as interfacial materials to modify metal electrodes is believed to be critical to achieve high efficiency (>10%) in PSCs with various materials systems.[18]

Received: July 1, 2013
Accepted: March 20, 2014
Published: March 20, 2014

Scheme 1. Synthesis of Monomers and WPFs

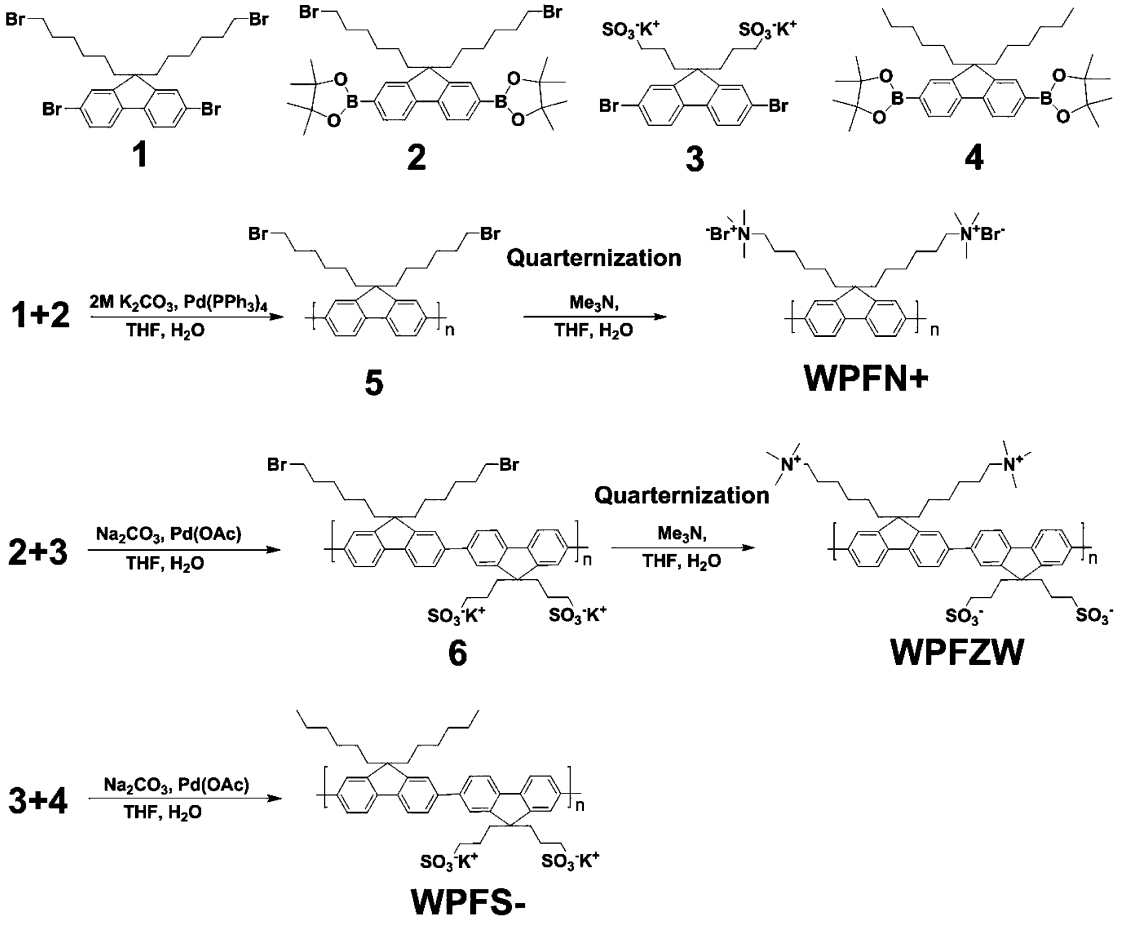

Despite the successful application of CPEs to I-PSCs, the influence of their ionic groups on device performance has not been extensively studied. In this paper, we synthesized water-soluble polyfluorene derivatives (WPFs) to gain insight into the influence of the ionic functionalities of WPFs on the role of the ITO cIFL in I-PSCs. Three WPFs with the same conjugated main chain, but with various ionic groups for side chains, were studied (see Scheme1): WPFN+, WPFZW, and WPFS-. A comparison between WPFN+ and WPFS- provided insight into the influence of charge reversal (cationic ammonium vs anionic sulfonates), but the study of WPFZW offered a perspective on the influence of zwitterions (contemporaneously containing these reverse charges). The modification of the work-function of ITO was significant and the device performance of I-PSCs was strongly dependent on the types of ionic side groups of the WPFs.

2. EXPERIMENTAL SECTION

2.1. Materials. All reagents and solvents were purchased from Aldrich, TCI Chemical Co., and Strem Chemicals Inc., and were used without further purification. 2,7-Dibromo-9,9-bis(6-bromohexyl)-9*H*-fluorene (**1**), 2,7-bis(4,4,5,5-tetramethyl-1,3,2-dioxaborolan-2-yl)-9,9-bis(6′-bromohexyl)fluorene (**2**), 2,7-dibromo-9,9-bis(4-sulfonatobutyl)fluorene dipotassium (**3**), and 2,7-bis(4,4,5,5-tetramethyl-1,3,2-dioxaborolan-2-yl)-9,9-dihexylfluorene (**4**) were prepared according to a procedure found in the literature.[19,20]

*Poly[9,9-bis(6-bromohexyl)-9H-fluorene] (**5**).* 2,7-Dibromo-9,9-bis(6-bromohexyl)-9*H*-fluorene (**1**) (0.325 g, 0.5 mmol), 2,7-bis(4,4,5,5-tetramethyl-1,3,2-dioxaborolan-2-yl)-9,9-bis(6′-bromohexyl)fluorene (**2**) (0.372 g, 0.5 mmol), 5 mL of 2M K_2CO_3, and 15 mL of toluene were degassed. After being purged with nitrogen for 30 min, $Pd(pph_3)_4$ (0.028 g) was added into the reaction mixture. The mixture was stirred at 100 °C for 72 h. After cooling to room temperature, the mixture was precipitated by being dropped into a stirred ethanol/HCl solution (1:1 v/v). The polymer was purified with methanol and hexane using Soxhlet extraction and extracted with chloroform. The solution was precipitated into methanol and filtered to afford poly[9,9-bis(6-bromohexyl)-9*H*-fluorene] (**5**). After drying in vacuum, the final polymer was obtained as a yellow powder (0.392 mg, 80%).^{1}H NMR ($CDCl_3$-*d*, 400 MHz): δ (ppm) 7.80-7.71 (br, 6H, aromatic H), 3.24-3.20 (br, 4H, alkyl side chain H), 1.04-2.03 (br, 16H, alkyl side chain H), 0.48-0.55 (br, 4H, alkyl side chain H). Anal. Calcd (%) for $(C_{25}H_{30}Br_2)_n$: C, 60.99; H, 6.55. Found: C, 61.12; H, 6.25.

Poly[9,9-bis(6′-(N,N,N-trimethylammonium)hexyl)fluorene]-bromide (WPFN+). Quarternization. The compound (**5**) was dissolved in tetrahydrofuran (THF). Trimethylamine (Me_3N) solution was added to the solution, which was then stirred at room temperature. The solubility of the ionic polymer decreased in the THF, and it precipitated during this period. DI was added to the solution in order to dissolve the precipitate. The process was repeated 4 times over a period of 2 days. The solution was evaporated and the residue was redissolved in MeOH. The ionic polymer was precipitated from ether.

Dialysis. Excess catalysts, impurities, and low molecular weight compounds can be removed using special purification techniques that differ from neutral polymers. Dialysis involves the separation of lower molecular weight compounds from macromolecular solutions via passage through membranes. After ionic polymers were dried under vacuum, they were dissolved in DI and then placed in a size-selective permeable tube (Spectra/Por Cellulose Ester Membrane with a cutoff molecular weight of 2000). The tube was put into a beaker filled with

stirred DI. For efficient dialysis, the DI in the beaker was changed every 3−6 h until low molecular weight molecules would no longer pass through (about 3−4 days). The dialyzed solution was frozen by liquid nitrogen and dried for 2−3 days in vacuum. The freeze-dried final product was obtained as a chrome yellow powder (180 mg, 37%). The final product polymers were dried in vacuum at 80 °C for 24 h. Each polymer was dialyzed for 3 days using a membrane with a 2000 molecular weight cutoff. Anal. Calcd (%) for $(C_{31}H_{48}Br_2N_2)_n$: C, 60.98; H, 8.25; N, 4.59. Found: C, 53.64; H, 6.92; N, 3.87.

Potassium Poly[9,9-bis[6′-(N,N,N-trimethylammonium)hexyl]-fluorene-alt-co-bis(3′-sulfonatopropyl)]bromide (WPFZW). 2,7-Bis-(4,4,5,5-tetramethyl-1,3,2-dioxaborolan-2-yl)-9,9-bis(6′-bromohexyl)-fluorene (**2**) (0.372 g, 0.5 mmol), 2,7-dibromo-9,9-bis(4-sulfonatobutyl)fluorene dipotassium (**3**) (0.322 g, 0.5 mmol), 5 mL of 2 M K_2CO_3, and 15 mL of distilled THF were degassed. After being purged with nitrogen for 30 min, $Pd(pph_3)_4$ (0.028 g) was added to the reaction mixture. The mixture was stirred at 100 °C for 72 h, and a solution of Me_3N was added to the solution, which was then stirred at 70 °C. DI was added to the solution in order to dissolve the precipitate. The process was repeated 4 times in 1 day. After cooling to room temperature, the mixture was dissolved in DI. The precipitate that was undissolved by the DI was then filtered off. The solution was evaporated and the residue was redissolved in DI. The ionic polymer was precipitated from ether. After quarternization using Me_3N, the polymer was purified by the same dialysis method as that of WPFN+. After freeze-drying, the final polymer was obtained as a light yellow powder (250 mg, 50%). ^{1}H NMR (D_2O-d, 400 MHz): δ (ppm) 7.88-7.73 (br, 12H, aromatic H), 3.02-3.24 (br, 22H, alkyl side chain H), 2.23 (br, 4H, alkyl side chain H), 1.58-1.19 (br, 24H, alkyl side chain H), 0.73 (br, 4H, alkyl side chain H). Anal. Calcd (%) for $(C_{52}H_{70}K_2N_2O_6S_{22})_n$: C, 55.60; H, 6.46; N, 2.49; O, 8.55; S, 5.71. Found: C, 55.45; H, 6.60; N, 2.49; O, 9.08; S, 6.01.

Potassium Poly[9,9-bis(3′-sulfonatopropyl)fluorene-alt-(9,9-dihexylfluorene)] (WPFS-). 2,7-Dibromo-9,9-bis(4-sulfonatobutyl)-fluorene dipotassium (**3**) (0.322 g, 0.5 mmol), 2,7-bis(4,4,5,5-tetramethyl-1,3,2-dioxaborolan-2-yl)-9,9-dihexylfluorene (**4**) (0.257 g, 0.5 mmol), Na_2CO_3 (0.5 g, 4.27 mmol), 23.5 mL of DI, 10 mL of DMF, and 7.5 mL of THF were degassed. After being purged with nitrogen for 30 min, $Pd(OAc)_2$ (0.007g) was added into the reaction mixture. The mixture was stirred at 100−110 °C for 60 h. After cooling to room temperature, the precipitated Pd particles were removed by filtration using a glass filter, and then the entire solution was evaporated and dried under vacuum. Acetone was added to the dried solid. The solution was separated by filtration. The filtrate polymer was dried under vacuum. The final polymer was purified using the same dialysis method as that of WPFN+. The final polymer was obtained after freeze-drying as a light green powder (215 mg, 49%). ^{1}H NMR (MeOH-*d*, 400 MHz): δ (ppm) 7.87-7.34 (br, 12 H, aromatic H), 2.66-0.68 (br, 38H, alkyl side chain H). Anal. Calcd (%) for $(C_{48}H_{58}K_2O_6S_2)_n$: C, 65.86; H, 6.91; O, 10.97; S, 7.33. Found: C, 64.12; H, 6.22; O, 10.69; S, 7.14.

2.2. Measurements. The ^{1}H NMR was obtained using a JEOL JNM-LA300WB at 400 MHz with tetramethylsilane as a reference. The UV−visible absorption spectra were recorded using a Perkin-Elmer Lambda 12 UV−visible spectrophotometer (HP 8453). Elemental analyses were performed on a Flash2000 (CE Instrument, Italy). Molecular weights of the WPFZW were obtained on a Waters GPC system using a calibration curve of poly(methyl methacrylate) (PMMA) standards, with DMSO (0.01 M LiBr at 80 °C) as the eluent. Molecular weights of the neutral polymer before quarternization of the WPFN+ were obtained on a GPC (Futecs, NS2001) using a calibration curve of polystyrene standards, with THF as the eluent. Cyclic voltammetry (CV) was carried out for 0.1 M Bu_4NClO_4 in acetonitrile (CH_3CN) using a potentiostat (Eco Chemies, AUTO-LAB) at a scan rate of 100 mV/s at room temperature. An ITO glass, a silver wire, and a platinum wire were used as the working, reference, and counter electrodes, respectively. The reference electrode was calibrated using 0.1 M ferrocene. Working electrodes were prepared by spin coating using WPF solutions. The surface energy of P3HT, $PC_{61}BM$, P3HT:$PC_{61}BM$, and ITO modified with WPFs with and without annealing was evaluated by the contact angle measurement using two different liquids, DI and diiodomethane (DIM) (Aldrich), as probe liquids. Ultraviolet photoelectron spectroscopy (UPS) and X-ray photoelectron spectroscopy (XPS) data were obtained using a Kratos to measure the work-function of a metal, onto which WPFs had been spin-coated. The characteristics for surface roughness and morphology of the ITO and WPFs on ITO were obtained using atomic force microscopy (AFM, Digital Instruments Nanoscope IV in tapping mode). A pH meter (Thermo Scientific Orion) was used to obtain the pH of WPF solution.

2.3. Fabrication and Characterization of Inverted Polymer Solar Cells. To fabricate the device, indium tin oxide (ITO)-coated glass substrates (Samsung Corning Co., Ltd.) were cleaned, dried in an oven, and treated by UV-ozone for 10 min. WPFN+, WPFZW, and WPFS-, dissolved in methanol, and DI and DI at 0.55 mg/mL, were spin-coated onto the ITO substrate under air (pH = 5.8 for WPFN+ sol, pH = 6.2 for WPFZW, and pH = 3.2 for WPFS-). As the active layer, a blend solution film of 30 mg of P3HT (Rieke Metals) and 15 mg of $PC_{61}BM$ (Nano-C) in 2 mL of chlorobenzene (CB) was then spin-coated onto WPFs, at ∼60 nm, followed by drying at 110 °C for 10 min in a N_2-filled glove box. A diluted solution of PEDOT:PSS in IPA was spin-coated onto the active layer at a thickness of ∼16 nm, followed by drying at 120 °C for 10 min under air. Under vacuum at 10^{-6} Torr, 100 nm of silver (Ag) was thermally deposited onto the PEDOT:PSS layer. After deposition of the Ag electrode, the devices were hot-plate-based post-annealed at 170 °C for 30 min. The devices had an area of 4.64 mm^2. Photocurrent−voltage (*J*−*V*) characteristics of the devices were measured using a Keithley 4200 instrument under an illumination of 100 mA cm^{-2} from a 1 KW Oriel solar simulator with an AM 1.5 G filter in a N_2-filled glove box. A calibrated silicon reference solar cell with a KG5 filter certified by the National Renewable Energy Laboratory (NREL) was used to confirm the measurement conditions.

3. RESULTS AND DISCUSSION

3.1. Synthesis of Monomers and Polymers. The synthetic route for polymers used in the present study is shown in Scheme 1. Monomers **1**, **2**, **3**, and **4** were synthesized according to a previously published method.[19] The precursor polymer (**5**) of WPFN+ was synthesized from monomers **1** and **2** via $Pd(PPh_3)_4$-catalyzed Suzuki coupling. The precursor polymer (**5**) was dissolved in organic solvents such as chloroform and THF, which enabled determination of the molecular weights of the polymers by gel permeation chromatography (GPC) with calibration of the polystyrene standards and THF as the eluent. The number-average molecular weight (M_n) of (**5**) was 14,000 with a polydispersity index (PDI) of 1.85. The quarternization of polymer (**5**) with Me_3N in THF/DI provided WPFN+. The final product was obtained by dialysis in a membrane with a cutoff of 2000. WPFN+ was not soluble in most organic solvents such as THF or toluene but was completely soluble in methanol and partially soluble in water. Due to the strong aggregation tendency on the column fillers induced by the ionic groups on polymers,[21] obtaining the molecular weights of WPFN+ using GPC was unsuccessful, but the molecular weight of WPFN+ was comparable to its precursor polymer. WPFN+ was confirmed by elemental analysis (EA).

The precursor polymer of WPFZW was synthesized from monomers **2** and **3** via $Pd(OAc)_2$-catalyzed Suzuki coupling. The precursor polymer (**6**) of WPFZW was not separately precipitated, and polymer (**6**) was quarternized with Me_3N in the same batch following polymerization, and was then purified using the same dialysis method as that of WPFN+. WPFZW was not soluble in most organic solvents, as in the case of WPFN+, but was completely soluble in water and partially

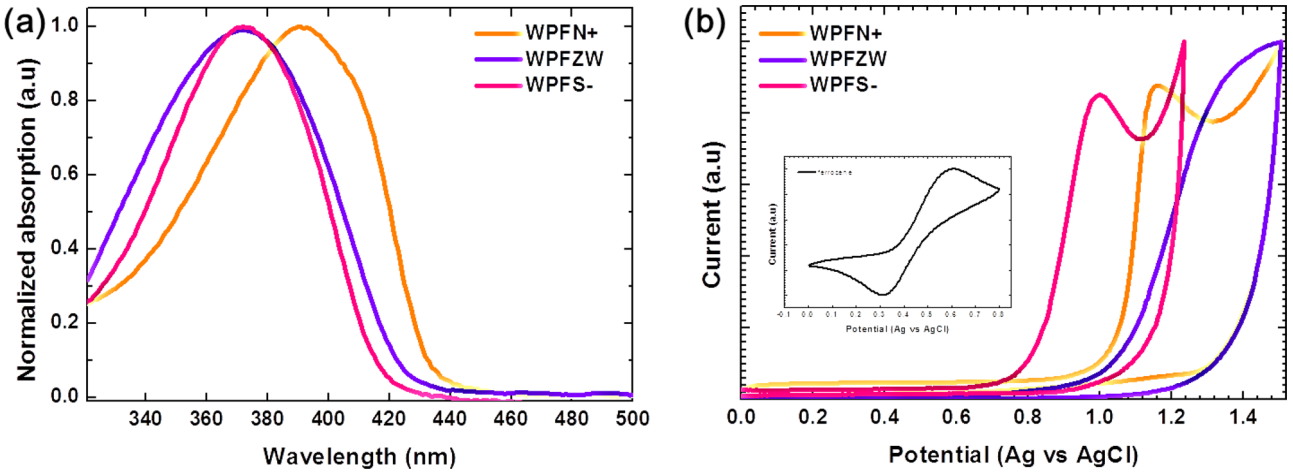

Figure 1. (a) Normalized UV−vis absorption spectra and (b) cyclic voltammetry of films of WPFN+, WPFZW, and WPFS-.

soluble in MeOH. When using GPC with calibration of the PMMA standards and DMSO and 0.01 M LiBr as the eluent at 80 °C, the M_n of WPFZW was 16,200, with a PDI of 1.22. WPFZW was confirmed by ^{1}H NMR and EA.

Synthesis of WPFS- was accomplished via the $Pd(OAc)_2$-catalyzed Suzuki coupling of monomers **3** and **4**. WPFS- was extracted from acetone and then purified by the same dialysis method as that of WPFN+. The solubility of WPFS- was limited in an organic solvent but was completely soluble in DI and partially soluble in DMSO and MeOH. The molecular weights of WPFS- could not be obtained using GPC for the same reason that applied in the case of WPFN+. WPFS- was confirmed by ^{1}H NMR and EA.

3.2. Optical and Electrochemical Properties. The optical properties of three WPFs are shown in Figure 1a. The UV−vis absorption spectra of the polymers were measured in film. Films were obtained by spin-coating WPFN+, WPFZW, and WPFS- in methanol and DI, respectively. WPFN+ film showed an absorption maximum (λ_{abs}) at 390 nm and an absorption onset (λ_{onset}) at 434 nm. In the case of WPFZW film, λ_{abs} and λ_{onset} appeared at 374 and 424 nm, respectively. WPFS- film showed λ_{abs} and λ_{onset} that appeared at 372 and 417 nm, respectively. The optical band gaps (E_g) of WFPN+, WPFZW, and WPFS- were 2.88, 2.92, and 2.97 eV, respectively. The E_g of WPFS- films were slightly higher than that of WFPN+ due to their shorter conjugation length. WPFs were similar in optical band gap to analogous polymers with a fluorene main chain, indicating that ionic side chains did not influence their optical properties.[22,23]

The HOMO levels of WPFN+, WPFZW, and WPFS- were obtained from the onsets of the oxidation potential (E_{ox}) when cyclic voltammetry was performed in 0.1 mol/L of Bu_3NClO_4 in a CH_3CN solution (Figure 1b). Three polymers were spin-coated onto ITO to serve as a working electrode. A Pt wire was used as the counter electrode and Ag wire was used as the reference electrode. The HOMO levels of WPFN+, WPFZW, and WPFS- were −5.37, −5.27, and −5.15 eV, respectively. The LUMO levels were calculated from the HOMO level and E_g. The optical properties and electrochemical properties are summarized in Table 1.

3.3. Surface Characterization of ITO Modified with WPFs. To characterize the surface of ITO modified with WPFs, its work-function was investigated using UPS (Figure 2a and Table 2). The high binding energy cutoffs (E_{cutoff}) for WPF

Table 1. Summary of UV−vis Absorption and Electrochemical Properties of WPFs

polymer	λ_{max} (nm)	λ_{onset} (nm)	E_g[a] (eV)	HOMO[b] (eV)	LUMO[c] (eV)
WPFN+	390	434	2.88	−5.37	−2.49
WPFZW	374	424	2.92	−5.27	−2.35
WPFS-	372	417	2.97	−5.15	−2.18

[a]Estimated from the onset wavelength of the optical absorption in the solid state film. [b]Calculated from HOMO (eV) = −4.8 − (E_{onset} − $E_{1/2}$(Ferrocene)). [c]Calculated from the HOMO level and optical band gap.

films spin-coated onto an ITO are shown in Figure 2a. The calculated work-function of cleaned and UV-ozone-treated ITO for 10 min was 4.53 eV. Even for thin WPF films (∼2 nm) spin-coated onto ITO, there was a significant shift of the E_{cutoff} toward higher energy for WPFN+ and WPFZW, and for WPFS- we observed a shift of the E_{cutoff} toward lower energy that corresponded to the total vacuum level (E_{vac}) shift between the WPFs and the ITO. The shift of E_{vac}, indicated that an interfacial dipole existed at the WPF/ITO interfaces, and was equivalent to subtracting the work-function of ITO from the difference between the E_{vac} of WPF film and the Fermi energy (E_f) of ITO.[23,24] Figure 2b shows the possible energy diagrams of the WPF/ITO interfaces in the presence of the interfacial dipole, according to the UPS data. There was a significant difference in the electronic properties of the WFPS-/ITO interfaces. WPFN+ and WPFZW reduced the work-function of ITO by 0.43 and 0.74 eV, respectively, while WPFS- slightly increased the work-function of ITO by 0.25 eV. Those results indicated that an interfacial dipole at the ITO/WPFs could be formed as a function of the ionic groups and the counter ion. To observe the change in ITO surface-modified WPFs, WPFs on ITO were characterized using AFM. As shown as Figure S1a, AFM images revealed no differences between bare ITO and ITO modified with WPFs.

To confirm the existence of WPFs on ITO with regard to the work-function modification of ITO, the XPS spectra for WPFs/ITO were measured. Figure 3 shows the In 3d and O 1s XPS spectra of bare ITO and ITO modified by WPFs. Although peaks for ITO still exist, due to very thin WPFs (2 nm), we found that the In 3d peaks for WPFN+ and WPFZW were shifted to a lower binding energy by 0.25 and 0.78 eV, respectively, while the peak for WPFS- was shifted to a higher

dx.doi.org/10.1021/am500708k | ACS Appl. Mater. Interfaces 2014, 6, 6227−6236

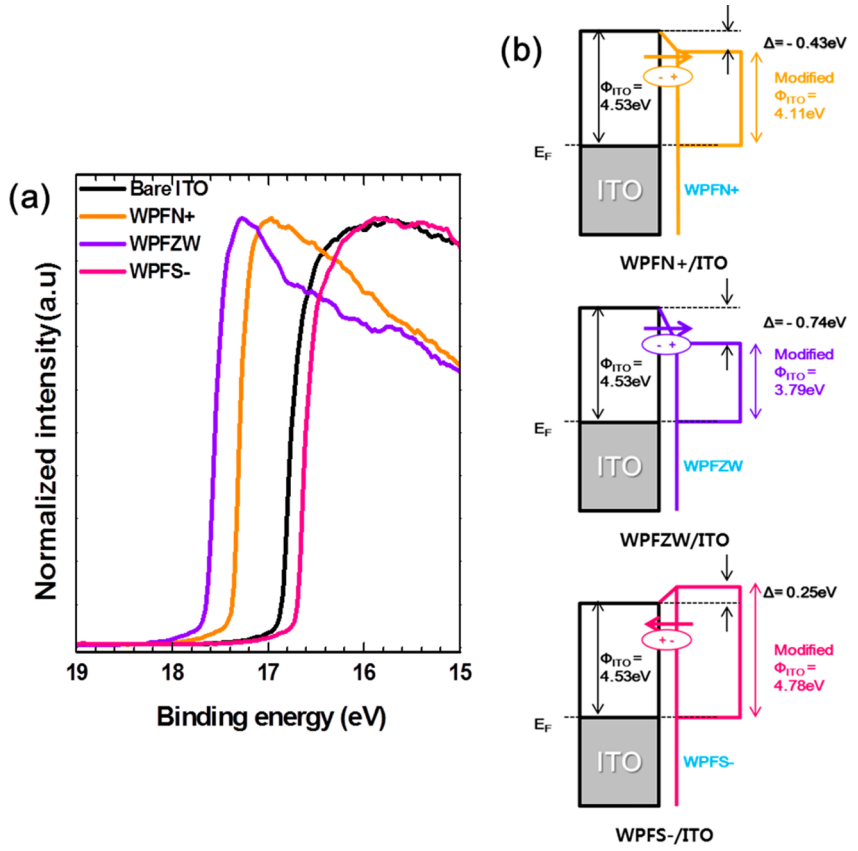

Figure 2. (a) UPS spectra of WPFs spin-coated onto ITO and (b) energy diagram of the WPF/ITO interfaces.

Table 2. Work Function (Φ), Contact Angle, and Surface Energy of ITO Modified with WPFs

			contact angle (°)		surface energy[e] (mJ/m^2)		
surface	ΔΦ (eV)[a]	Φ_{ITO} (eV)[b]	Θ_{DI}[c]	Θ_{DIM}[d]	γ_s^p	γ_s^d	γ
UV-ozone ITO	-	4.53	29.9	27.5	26.2	45.2	71.4
WPFN+	−0.43	4.11	54.8	16.6	12.1	48.7	60.8
WPFZW	−0.74	3.79	26.0	13.1	25.8	49.5	75.3
WPFS-	0.25	4.78	46.8	25.4	17.2	46.0	63.2

[a]ΔΦ values are for the difference in the work function. [b]Modified work function of ITO. [c,d]Contact angle of a water droplet (θ_{DI}) and a diiodomethane droplet (θ_{DIM}) on WPFs spin-coated on ITO with thermal annealing at 170°C. [e]The surface energies were determined from contact angle measurements performed with water and diiodomethane as probe liquids by applying the Owens-Wendt geometric mean equation: $(1+\cos\theta)\gamma_L = 2(\gamma_S^d\gamma_L^d)^{1/2} + 2(\gamma_S^p\gamma_L^p)^{1/2}$, where γ_S and γ_L are the surface energies of the substrate and probe liquid, respectively, and the superscripts d and p refer to the dispersion and polar components of the surface energy, respectively. The total energy (γ) is the sum of γ_s^p and γ_S^d.

binding energy by 0.16 eV (ΔΦ in Table 2 is apparently related to the extent of the binding energy shift of the WPFs). Similar shift trends were also observed for the O 1s XPS spectra of ITO modified by WPFs. These chemical shifts in the peaks of binding energies suggest the following: (i) the interaction of quaternary ammonium ions ($-N(CH_3)_3^+$), sulfonate ions ($-SO_3^-$), bromide ion (Br^-), and potassium ion (K^+) with ITO surface and (ii) the chemical shift were quite dependent on the type of WPFs studied here, as shown Figure 3. The O 1s XPS spectra include various oxygen species, which could be the result of the following: (1) oxide of ITO,[25,26] (2) $-SO_3^-$ for WPFZW and WPFS-, (3) hydrogen bonding,[27−29] and (4) electrostatic interaction of WPFs onto the ITO and others (complicated fitting data not shown). The existence of counter ions (Br^- and K^+) in WPFs is also confirmed in Figure S1b and c.[24] (When we performed dialysis for more than 2 days, the intensity of K^+ experimentally disappeared, while the intensity Br^- just decreased compared with WPFZW without dialysis. Those results imply that the negative $-SO_3^-$ is compensated for by positive $-N(CH_3)_3^+$ and $-N(CH_3)_3^+$ and that Br^- pairs still exist.) Hence, these XPS data confirmed strong interaction between WPFs and ITO, which would be a critical factor for determining the dipole moment at the WPF/ITO interfaces and the surface energy of WPFs on ITO.[30,31]

To characterize the effect of WPFs on the surface energy of ITO, the contact angles with a water droplet were measured for UV-ozone-treated ITO, and for ITO modified with WPFs without thermal annealing. The contact angles for WPFN+, WPFZW, and WPFS- were 29.9°, 39.1°, 6.3°, and 36°, respectively (see Table S1 and Figure S2). The precursor polymers of WPFN+ and WPFZW were almost quaternized (see Figure S1b and c). That result indicates that most of their side chains would be charged. The contact angle of ITO modified with WPFZW was the smallest, which equates to a hydrophilic surface with more ionic groups exposed to air, compared with an ITO surface modified with WPFN+ and WPFS-. When ITO modified with WPFs were thermal annealed under the same conditions as device fabrication, all the contact angles were increased. It is suspected that the ionic side chains of the WPFs were moved down the ITO or

dx.doi.org/10.1021/am500708k | ACS Appl. Mater. Interfaces 2014, 6, 6227−6236

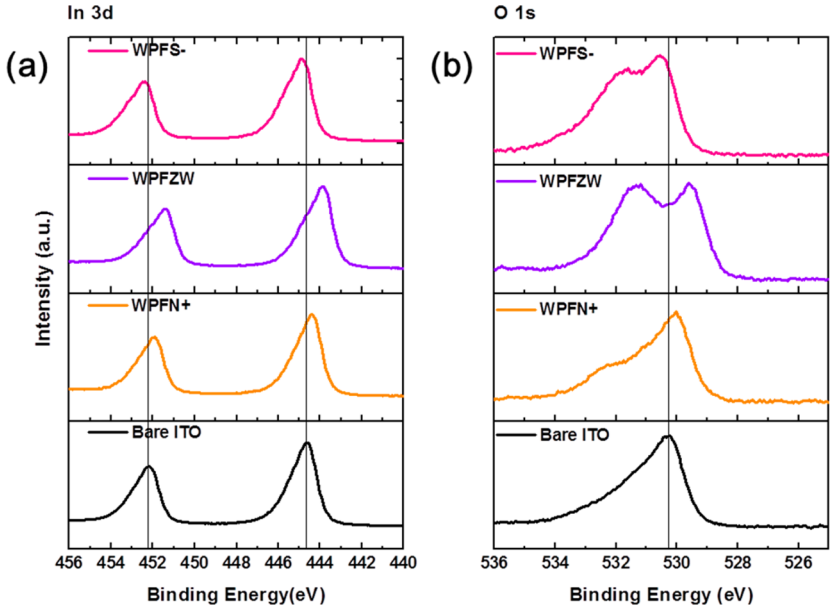

Figure 3. XPS spectra of WPFs spin-coated onto ITO: (a) In 3d; (b) O 1s.

nonpolar aromatic backbone of the WPFs faced upward to the surface via thermal annealing (see Figure S2 and Figure 5). In addition, the surface energy of ITO modified with WPFs was determined from the contact angle using DI and diiodomethane (DIM) as probe liquids (see Figure S1 and Table S1).[32] Figure 4 shows that the surface energy for ITO-modified

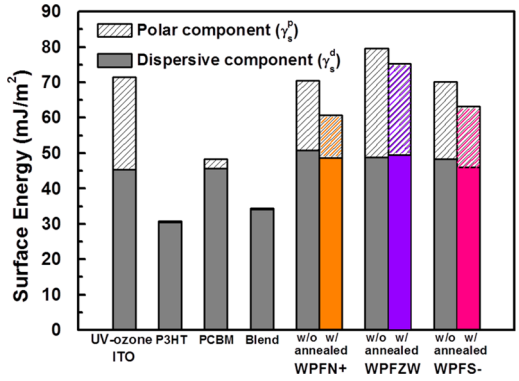

Figure 4. Surface energy distribution of UV-ozone treated ITO, P3HT, $PC_{61}BM$, P3HT:$PC_{61}BM$, and ITO modified WPFs with and without annealing at 170 °C for 30 min.

WPFs decreases when annealing at 170 °C for 30 min (the same condition as post-annealing). The polar components of the surface energy for WPFN+, WPFZW, and WPFS- were decreased by 7.5, 5, and 4.7 mJ/m^2, respectively. The dispersive components of the surface energy for all WPFs with and without annealing were similar, and the hydrophobic surface was maintained due to the aromatic backbone. As shown by the contact angle of a water droplet, the polar components of the surface energy for WPFZW with and without annealing were higher than those of WPFN+ and WPFS-.

To gain further insight into the surface of WPFs on ITO, we propose preferential orientation changes of WPFs onto ITO, based on changes in XPS data and in surface energy, as shown in Figure 5. We assumed that 1 layer of a WPF backbone was oriented with a orbital perpendicular to the substrate (mild plane-on orientation), considering 2 nm thickness of WPFs.[33] In Figure 5a(1), when WPF is spin-coated on ITO under the air, both ionic side chains and their counter ions (due to electrostatic paring) could be oriented toward the air for all WPFs. Since the polar components in surface energy of ITO modified with WPFs were decreased when WPFs annealed onto ITO under air, both of the more ionic side chains and their counter ions could be oriented toward ITO in Figure 5a(2). Hence, the O 1s binding energy peaks of WPFs in Figure 3b show many components. Additionally, if we assumed the orientation of WPFs is possible when an active layer was spin-coated onto WPFs during the fabrication of I-PSCs, more hydrophilic ionic side chains and their counter ions of WPFs were located on the ITO. This can be explained by previously reported studies.[33,34] Based on these studies, Figure 5a(3) shows how more ionic side chains and their counter ions could be located to ITO, in the present study, compared with Figure 5a(1) and (2), because WPFs were beneath the hydrophobic P3HT:$PC_{61}BM$ in this case.

We also suggest a possible orientation scheme of the WPFs when dipole is formed at the WPF/ITO interfaces in Figure 5b, based on the characterizations mentioned above. For the WPFN+/ITO, the direction of the dipole moments pointed outward from the ITO in order to reduce the ITO work-function, as shown in Figure 2b. This possible orientation for the dipole formation can be explained by recent studies.[10] Since we observed the negative counter ion Br^- of WPFN+ in XPS data, Br^- could be preferentially located to ITO due to the higher dielectric constant of ITO[10,33] and the positive -$N(CH_3)_3^+$ could be electrostatically paired with Br^-, resulting in dipole formation that was consistent with previous studies. For WPFZW/ITO, the direction of the dipole moment was the same as that of WPFN+, but the possible orientation could be explained differently due to the alternation of $N(CH_3)_3^+$ and $-SO_3^-$ in WPFZW. The side chains with $-SO_3^-$ (not paired with K^+) can face toward ITO and the side chains with -$N(CH_3)_3^+$ can face upward towards the air, as shown in Figure 2b.

For WPFS-/ITO, the direction of the dipole moment points away from ITO, resulting in an increase in ITO work-function, as shown in Figure 2b. The existence of K^+ was uncertain

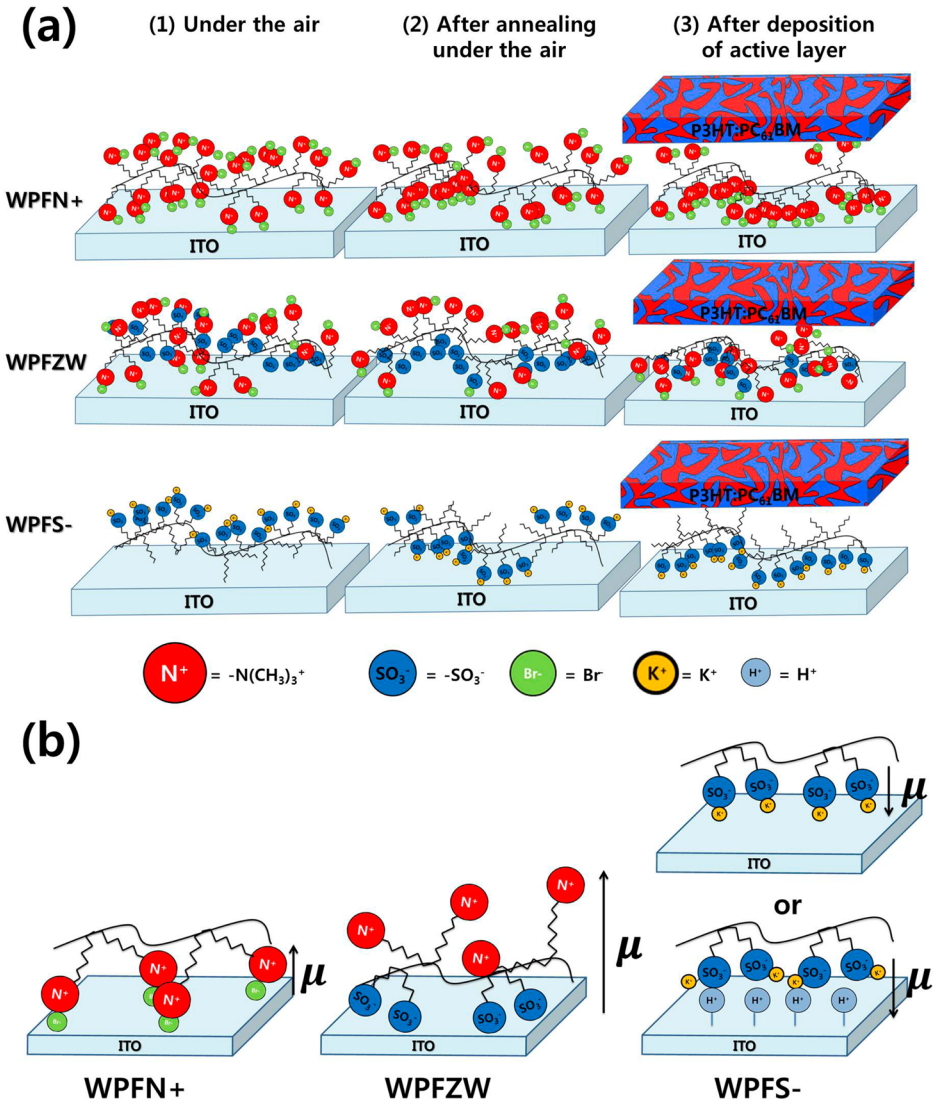

Figure 5. Schematic possible orientations of WPFs on ITO (a) under different conditions ((1) under the air, (2) after annealing under the air, (3) after deposition of active layer) and (b) the possible of dipole formation at WPFs/ITO.

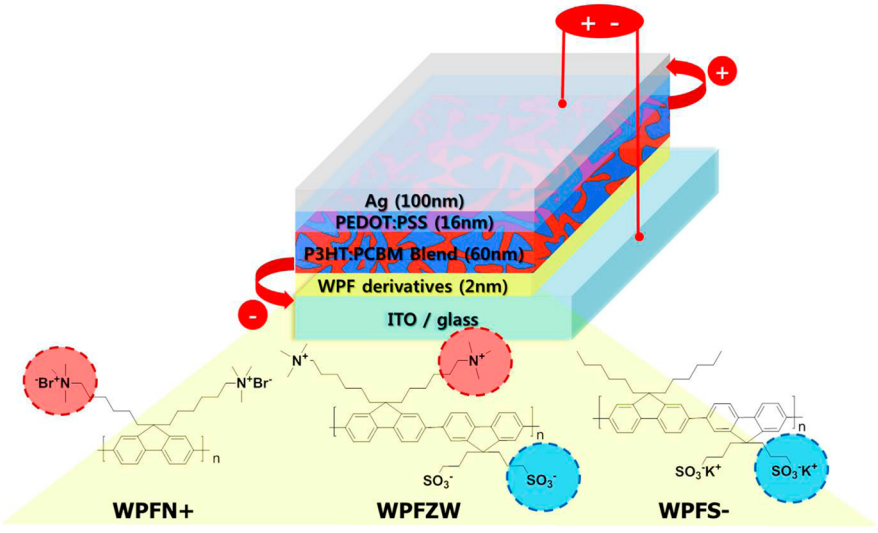

Figure 6. Structure of the inverted polymer solar cell with WPF derivatives.

dx.doi.org/10.1021/am500708k | ACS Appl. Mater. Interfaces 2014, 6, 6227−6236

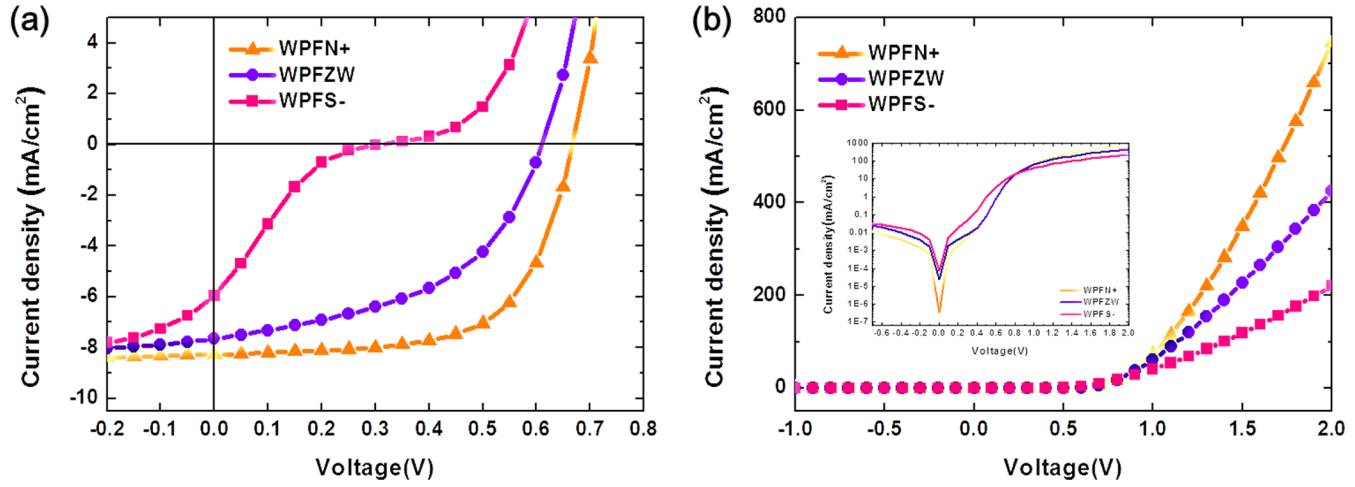

Figure 7. *J*–*V* characteristics of inverted polymer solar cells with WPFs as cathode interfacial layers (a) under illumination and (b) in the dark.

because the bare ITO also showed peaks of K^+. Hence, we suggested two possible orientations for WPFS- onto ITO: (1) mobile K^+ could be located to ITO, and $-SO_3^-$ could electrostatically pair with K^+; or (2) due to pH = 3.2 of WPFS- (0.5 mg/mL in DI), acid treatment could lead to the protonation of the ITO surface.[35] Although the exact orientation of the ionic groups in the side chains of WPFs remains poorly understood, the surface energy of ITO modified with WPFs can determine the wettability of the subsequently spin-coated layers of PSCs.[36]

3.4. Photovoltaic Performance. To investigate the properties of WPFs when using them as the ITO cIFL in I-PSCs, I-PSCs were fabricated with a device configuration of ITO/WPFs of (~2 nm)/P3HT:PC61BM (62 nm)/PEDOT:PSS (16 nm)/Ag (100 nm) (Figure 6). The thickness of the WPFs (~2 nm) was estimated via ellipsometer measurement and a thickness vs optical density calibration curve. The blended P3HT:PC_{61}BM chlorobenzene solution was spin-coated, followed by an evaporation of 100 nm of Ag in vacuum. After the deposition of the Ag electrode, the devices were post-annealed at 170 °C for 30 min according to our previous work.[11]

Figure 7a shows the *J*–*V* curves of the devices under 100 mW cm^{-2} illumination with AM 1.5 G. Figure 7b shows the *J*–*V* curves in the dark. Table 3 summarizes the photovoltaic parameters of the I-PSCs when using WPFs as the ITO cIFL in I-PSCs. The I-PSCs based on P3HT:PCBM with interfacial layers showed PCEs of 3–4% in previously reported studies.[11,16,25,26,34,36,38] We also fabricated I-PSCs with frequently used PFN, PEIE, and sol-gel ZnO as cIFL compared with our cIFL with various ionic functionalities (see Figure S4 and Table S2). In our system, the I-PSC devices without cIFL scarcely worked or exhibited PCE = 0.3% (data not shown). The devices with WPFN+ (with only positive $-N(CH_3)_3^+$) exhibited a photovoltaic performance of V_{oc} = 0.67 V, FF = 0.64, and PCE = 3.53%. Devices with WPFN+ significantly enhanced the V_{oc} by 0.67 V, compared with I-PSCs with other materials (V_{oc} range 0.61–0.65 V in Table S2). The results from the reduction of ITO work-function led to better electron transport and collection. In Figure 7b, the series resistance (R_s), which was associated with the resistance of the semiconductor bulk, the metal electrodes, and the metal/semiconductor interfaces, was calculated from an inverse slope in the dark *J*–*V* curves over the V_{oc}.[16,37,38] I-PSCs with WPFN+ showed the smallest R_s at 1.72 Ω cm^2 among I-PSCs with WPFs. In addition, as shown in the inset of Figure 7b, the I-PSCs with WPN+ had a smaller leakage current at negative voltages and low positive voltages. The shunt resistance (R_{sh}), relative to the recombination of charge carriers at the donor/acceptor interface and near electrodes,[14,30,31] was larger by one order of magnitude, compared with the R_{sh} of I-PSCs with WPFZW and WPFS-.

Table 3. Photovoltaic Performance of the Inverted Polymer Solar Cells with WPFs as Cathode Interfacial Layers

polymer	V_{oc} (V)	J_{sc} (mA/cm²)	FF	PCE (%)	R_{sh} (kΩ cm²)	R_s (Ω cm²)
WPFN+	0.67	8.27	0.64	3.53	120.77	1.72
WPFZW	0.61	7.65	0.49	2.28	49.93	2.99
WPFS-	0.30	5.94	0.17	0.31	16.12	6.10

The smaller R_s and larger R_{sh} were believed to have arisen from a reduction in the ITO work-function by the WPFN+ and the surface energy of WPFN+/ITO. As shown in Table 2, an Φ_{ITO} = 4.11 eV for WPFN+/ITO increased in the built-in potential between ITO and PEDOT:PSS/Ag electrodes and led to better matching between the ITO work-function and the LUMO of PCBM.[16] In addition, less hydrophilic surface of WPFN+/ITO than those of WPFZW and WPFS- could be beneficial for the subsequently coated active layer (the polar component for WPFN+ of 12.1 mJ/m^2 in Table S1), and when the active layer is spin-coated on WPFN+, more ionic side chains and counter ions located to ITO, as shown in Figure 5a, could enhance internal electric field in devices with WPFN+. From these results, WPFN+ as an effective ITO cIFL improved the extraction of electrons from active layers in the I-PSCs.

For I-PSCs with WPFZW (with both positive $-N(CH_3)_3^+$ and negative $-SO_3^-$), the device performance was not better than that of WPFN+. It was expected that WPFZW can give the most effective extraction of electrons among I-PSCs with WPFs because WPFZW significantly reduced the work-function of ITO (Φ_{ITO} = 3.79 eV). However, I-PSCs with WPFZW exhibited lower values for V_{oc} = 0.61 V, FF = 0.49, and PCE = 2.28%. It was obvious that the high dark current in the negative voltage region, which can be attributed to the leakage current, was increased and resulted in a relatively lower R_{sh} (49.93 kΩ cm^2). This result implies that much more of a

dx.doi.org/10.1021/am500708k | ACS Appl. Mater. Interfaces 2014, 6, 6227–6236

charge carrier interfacial recombination took place and resulted in a decrease in J_{sc}. The performance of I-PSCs with WPFZW did not match the reduction of ITO work-function, unlike the I-PSCs with WPFN+.

Such inconsistency could be explained by the surface energy and the orientation of WPFZW on ITO (see Figures 4, 5, and S2, Table S1). A WPFZW surface was not favorable to sequentially coated hydrophobic P3HT:$PC_{61}BM$, because even annealed WPFZW was quite hydrophilic (the polar component of 25.8 mJ/m^2). As shown in Figure 5a, if both negative ionic side chains and positive ionic side chains are contemporaneously located on ITO, when spin-coating the active layer onto WPFZW, electrostatic forces between polymer chains to keep apart from the active layer could induce a reorientation of WPFZW beneath the active layer. The reorientations of ionic side chains and remaining counter ions adjacent to ITO might induce an insufficient internal electric field of devices with WPFZW. The orientation of WPFZW at the buried interface beneath the active layer might result in device performance that was inconsistent with a reduction in the ITO work-function for the I-PSCs with WPFZW, even though it remains poorly understood.

The I-PSCs with WPFS- (with negative -SO_3^-) did not show good device performance (malfunction or S-shaped). WPFS- increased the work-function of ITO to Φ_{ITO} = 4.78 eV, which was unfavorable to the extraction of electrons from the active layer. As shown in Figure 7b, the injection current started to dominate at about 0.3 V in I-PSCs with WPFS-, due to a lower built-in potential in the device, whereas the dark current for the injection current started at about 0.6−0.7 V (corresponding to V_{oc}) in I-PSCs with WPFN+ and WPFZW. The performance of I-PSCs with WPFS- was consistent with the increase in the ITO work-function. We also fabricated normal devices, instead of inverted structure, using WPFS- as a replacement for PEDOT:PSS, based on an ITO work-function modified with WPFS- (see Figure S5 and Table S3). Contrary to our expectations, the normal devices using WPFS- exhibited poor performance, not consistent with a change in ITO work-function. It still remains a poorly understood characterization of WPFS- as an interfacial layer, which should be explored further.

4. CONCLUSIONS

In conclusion, we designed and synthesized three WPFs, WPFN+ (with quaternary ammonium ions), WPFZW (with quaternary ammonium and sulfonate ions), and WPFS- (with sulfonate ions), which were easily processed in orthogonal solvents for the subsequent coating of organic soluble layers in I-PSCs. WPFN+, a homopolymer with quaternary ammonium ion and counter Br^- ions on each side chain, reduced the ITO work-function to 4.11 eV as a result of the dipole moment at the WPFN+/ITO interface. WPFN+ spin-coated onto the ITO efficiently helped electron extraction to ITO and contributed to a higher V_{oc}, which resulted in a PCE of 3.53% in I-PSCs with WPFN+. WPFZW reduced the ITO work-function, but did not show good performance, and electron extraction to the ITO was poor in I-PSCs. In addition, WPFS- in I-PSCs was inefficient in extracting electrons from the active layer, because WPFS- increased the ITO work-function. These results show that there were substantial differences in the modification of the ITO work-function as a function of ionic groups on the side chains of WPFs, and, furthermore, device performance did not consistently correspond to the modification of ITO work-function probably due to more complicated WPF orientations at the buried interface beneath the active layer.

■ ASSOCIATED CONTENT

Supporting Information

Additional experimental details and additonal figures and tables as follows: AFM images of WPFs/ITO; images of (a) a water droplet and (b) a diiodomethane droplet on an ITO modified with WPFs; contact angle and surface energy of UV-ozone treated ITO, P3HT, $PC_{61}BM$, P3HT:$PC_{61}BM$ blend, and ITO modified WPFs; UV−vis spectra of the active layer on WPFs; the performance of inverted polymer solar cells with frequently used cathode interfacial layers; and the performance of normal structured solar cells with WPFS- as an anode interfacial layer. This material is available free of charge via the Internet at http://pubs.acs.org/.

■ AUTHOR INFORMATION

Corresponding Author

*E-mail: kimdy@gist.ac.kr.

Notes

The authors declare no competing financial interest.

■ ACKNOWLEDGMENTS

This work was supported by a National Research Foundation of Korea (NRF) grant funded by the Korea government (MSIP) (No. 2013-059210), (NRF-2009-C1AAA001-2009-0092950), NCRC grant (No. 2008-0062606, CELA-NCRC). We thank the Korea Basic Science Institute (KBSI) for UPS and XPS. We would like to thank the Nuclear Research and Development Program of Ministry of Science, ICT, and Future Planning of Korea for financial support.

■ REFERENCES

(1) Duarte, A.; Pu, K. Y.; Liu, B.; Bazan, G. C. Recent Advances in Conjugated Polyelectrolytes for Emerging Optoelectronic Applications. *Chem. Mater.* **2011**, *23*, 501−515.

(2) Lee, K.; Kim, H.-J.; Kim, J. Design Principle of Conjugated Polyelectrolytes to Make Them Water-Soluble and Highly Emissive. *Adv. Funct. Mater.* **2012**, *22*, 1076−1086.

(3) Lee, K.; Lee, J.; Jeong, J. E.; Kronk, A.; Elenitoba-Johnson, K. S. J.; Lim, M. S.; Kim, J. Conjugated Polyelectrolyte-Antibody Hybrid Materials for Highly Fluorescent Live Cell-Imaging. *Adv. Mater.* **2012**, *24*, 2479−2484.

(4) Jiang, H.; Taranekar, P.; Reynolds, J. R.; Schanze, K. S. Conjugated Polyelectrolytes: Synthesis, Photophysics, and Applications. *Angew. Chem., Int. Ed.* **2009**, *48*, 4300−4316.

(5) Feng, X. L.; Liu, L. B.; Wang, S.; Zhu, D. B. Water-Soluble Fluorescent Conjugated Polymers and their Interactions with Biomacromolecules for Sensitive Biosensors. *Chem. Soc. Rev.* **2010**, *39*, 2411−2419.

(6) Schanze, K. S.; Shellton, A. H. Functional Polyelectrolytes. *Langmuir* **2009**, *25*, 13698−13702.

(7) Søndergaard, R.; Helgesen, M.; Jørgensen, M.; Krebs, F. C. Fabrication of Polymer Solar Cells Using Aqueous Processing for All Layers Including the Metal Back Electrode. *Adv. Eng. Mater.* **2011**, *1*, 68−71.

(8) Lim, K.-G.; Choi, M.-R.; Kim, H.-B.; Park, J.; Lee, T.-W. High-Efficiency Polymer Photovoltaic Cells Using a Solution-Processable Insulating Interfacial Nanolayer: The Role of the Insulating Nanolayer. *J. Mater. Chem.* **2012**, *22*, 25148−25153.

(9) Chen, L.; Xie, C.; Chen, Y. Influences of Charge of Conjugated Polymer Electrolytes Cathode Interlayer for Bulk-Heterojunction Polymer Solar Cells. *Org. Electron.* **2013**, *14*, 1551−1561.

(10) Lee, B.; Jung, I.; Woo, H.; Shim, H.-K.; Kim, G.; Lee, K. Multi-Charged Conjugated Polyelectrolytes as a Versatile Work Function Modifier for Organic Electronic Devices. *Adv. Funct. Mater.* **2014**, *24*, 1100−1108.
(11) Kang, R.; Oh, S.-H.; Na, S.-I.; Kim, T.-S.; Kim, D.-Y. Investigation into the Effect of Post-Annealing on Inverted Polymer Solar Cells. *Sol. Energy Mater. Sol. Cells* **2014**, *120*, 131−135.
(12) Po, R.; Carbonera, C.; Bernardi, A.; Camaioni, N. The Role of Buffer Layers in Polymer Solar Cells. *Energy Environ. Sci.* **2011**, *4*, 285−310.
(13) Guan, X.; Zhang, K.; Huang, F.; Bazan, G. C.; Cao, Y. Amino N -Oxide Functionalized Conjugated Polymers and their Amino-Functionalized Precursors: New Cathode Interlayers for High-Performance Optoelectronic Devices. *Adv. Funct. Mater.* **2012**, *22*, 2846−2854.
(14) Gong, X. Toward High Performance Inverted Polymer Solar Cells. *Polymer* **2012**, *53*, 5437−5448.
(15) Yang, T. B.; Wang, M.; Duan, C. H.; Hu, X. W.; Huang, L.; Peng, J. B.; Huang, F.; Gong, X. Inverted Polymer Solar Cells with 8.4% Efficiency by Conjugated Polyelectrolyte. *Energy Environ. Sci.* **2012**, *5*, 8208−8214.
(16) Na, S. -I.; Kim, T. -S.; Oh, S. -H.; Kim, J.; Kim, S. -S.; Kim, D. -Y. Enhanced Performance of Inverted Polymer Solar Cells with Cathode Interfacial Tuning via Water-Soluble Polyfluorenes. *Appl. Phys. Lett.* **2010**, *97*, 223305.
(17) Lee, T. -W.; Lim, K. -G.; Kim, D. -H. Approaches Toward Efficient and Stable Electron Extraction Contact in Organic Photovoltaic Cells: Inspiration from Organic Light-Emitting Diodes. *Electron. Mater. Lett.* **2010**, *6*, 41−50.
(18) Helgesen, M.; Søndergaard, R.; Krebs, F. C. Advanced Materials and Processes for Polymer Solar Cell Devices. *J. Mater. Chem.* **2010**, *20*, 36−60.
(19) Oh, S. -H.; Na, S. -I.; Nah, Y. -C.; Vak, D.; Kim, S. -S.; Kim, D. -Y. Novel Cationic Water-Soluble Polyfluorene Derivatives with Ion-Transporting Side Groups for Efficient Electron Injection in PLEDs. *Org. Electron.* **2007**, *8*, 773−783.
(20) Oh, S. -H.; Na, S. -I.; Jo, J.; Lim, B.; Vak, D.; Kim, D. -Y. Water-Soluble Polyfluorenes as an Interfacial Layer Leading to Cathode-Independent High Performance of Organic Solar Cells. *Adv. Funct. Mater.* **2010**, *20*, 1977−1983.
(21) Huang, F.; Wu, H. B.; Wang, D. L.; Yang, W.; Cao, Y. Novel Electroluminescent Conjugated Polyelectrolytes Based on Polyfluorene. *Chem. Mater.* **2004**, *16*, 708−716.
(22) Huang, F.; Zhang, Y.; Liu, M. S.; Jen, A. K. Y. Electron-Rich Alcohol-Soluble Neutral Conjugated Polymers as Highly Efficient Electron-Injecting Materials for Polymer Light-Emitting Diodes. *Adv. Funct. Mater.* **2009**, *19*, 2457−2466.
(23) Seo, J. H.; Nguyen, T. Q. Electronic Properties of Conjugated Polyelectrolyte Thin Films. *J. Am. Chem. Soc.* **2008**, *130*, 10042−10043.
(24) Seo, J. H.; Yang, R. Q.; Brzezinski, J. Z.; Walker, B.; Bazan, G. C.; Nguyen, T. Q. Electronic Properties at Gold/Conjugated-Polyelectrolyte Interfaces. *Adv. Mater.* **2009**, *21*, 1006−1011.
(25) Sun, K.; Zhang, H.; Ouyang, J. Indium Tin Oxide Modified with Sodium Compounds as Cathode of Inverted Polymer Solar Cells. *J. Mater. Chem.* **2011**, *21*, 18339−18346.
(26) Sun, K.; Zhao, B.; Kumar, A.; Zeng, K.; Ouyang, J. Highly Efficient, Inverted Polymer Solar Cells with Indium Tin Oxide Modified with Solution-Processed Zwitterions as the Transparent Cathode. *Appl. Mater. Interfaces* **2012**, *4*, 2009−2017.
(27) Wu, L.; Jasinski, J.; Krishnan, S. Carboxybetaine, Sulfobetaine, and Cationic Block Copolymer Coatings: A Comparison of the Surface Properties and Antibiofouling Behavior. *J. Appl. Polym. Sci.* **2012**, *124*, 2154−2170.
(28) Krienke, H.; Vlachy, V.; Ahn-Ercan, G.; Bako. Modeling Tetraalkylammonium Halide Salts in Water: How Hydrophobic and Electrostatic Interactions Shape the Thermodynamic Properties. *J. Phys. Chem. B* **2009**, *113*, 4360−4371.
(29) Koller, J.; Grdadolnik, J.; Hadzi, D. Tetramethylammonium as Proton Donor in Hydrogen Bonding: An ab Initio and Infrared Study. *J. Mol. Struct. (Theochem)* **1992**, *259*, 199−209.
(30) Jea, S.H.; Kim, S.H.; Ko, J.H.; Yoon, Y.S. Study on Work Function Change of ITO Modified by Using a Self-Assembled Monolayer for Organic based Devices. *J. Kor. Phys. Soc.* **2006**, *49*, 2034−2039.
(31) Paramonov, P. B.; Paniagua, S. A.; Hotchkiss, P. J.; Jones, S. C.; Armstrong, N. R.; Marder, S. R.; Bredas, J.-L. Theoretical Characterization of the Indium Tin Oxide Surface and of Its Binding Sites for Adsorption of Phosphonic Acid Monolayers. *Chem. Mater.* **2008**, *20*, 5131−5133.
(32) Jung, G. H.; Lim, K.-G.; Lee, T.-W.; Lee, J.-L. Morphological and Electrical Effect of an Ultrathin Iridium Oxide Hole Extraction Layer on P3HT:PCBM Bulk-Heterojunction Solar Cells. *Sol. Energy Mater. Sol. Cells* **2011**, *95*, 1146−1150.
(33) Park, J.; Yang, R.; Hoven, C.; Gacrcia, A.; Fischer, D.; Nguyen, T.-Q.; Bazan, G. C.; DeLongchamp, D.M. Structural Characterization of Conjugated Polyelectrolyte Electron Transport Layers by NEXAFS Spectroscopy. *Adv. Mater.* **2008**, *20*, 2491−2496.
(34) Xie, C.; Chen, L.; Chen, Y. Electrostatic Self-Assembled Metal Oxide/Conjugated Polyelectrolytes as Electron-Transporting Layers for Inverted Solar Cells with High Efficiency. *J. Phys. Chem. C* **2013**, *117*, 24804−24814.
(35) Steim, R.; Kogler, F. R.; Brabec, C. Interface Materials for Organic Solar Cells. *J. Mater. Chem.* **2010**, *20*, 2499−2512.
(36) Bulliard, X.; Ihn, S.-G.; Yun, S.; Kim, Y.; Choi, D.; Choi, J.-Y.; Kim, M.; Sim, M.; Park, J.-H.; Choi, W.; Cho, K. Enhanced Performance in Polymer Solar Cells by Surface Energy Control. *Adv. Funct. Mater.* **2010**, *20*, 4381−4387.
(37) Servaites, J. D.; Ratner, M. A.; Marks, T. Organic Solar Cells: A New Look at Traditional Models. *J. Energy Environ. Sci.* **2011**, *4*, 4410−4422.
(38) Hau, S. K.; Yip, H. L.; Acton, O.; Baek, N. S.; Ma, H.; Jen, A. K. Y. Interfacial Modification to Improve Inverted Polymer Solar Cells. *J. Mater. Chem.* **2008**, *18*, 5113−5119.